IEEE Photonics Journal
An IEEE Photonics Society Publication

Theoretical Analysis of Heat Distribution in Raman Fiber Lasers and Amplifiers Employing Pure Passive Fiber

Volume 12, Number 6, December 2020

Yizhu Chen
Tianfu Yaoyaotianfumary@163.com
Hu Xiao
Jinyong Leng
Pu Zhou

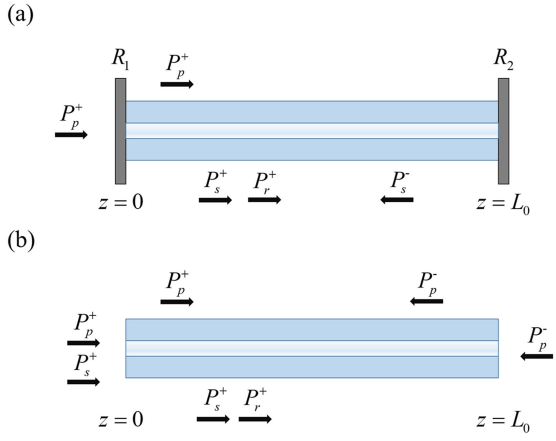

DOI: 10.1109/JPHOT.2020.3038350

Theoretical Analysis of Heat Distribution in Raman Fiber Lasers and Amplifiers Employing Pure Passive Fiber

Yizhu Chen, Tianfu Yao, Hu Xiao, Jinyong Leng, and Pu Zhou

College of Advanced Interdisciplinary Studies, National University of Defense Technology, Changsha 410073, China

DOI:10.1109/JPHOT.2020.3038350

Manuscript received August 23, 2020; revised November 1, 2020; accepted November 11, 2020. Date of publication November 16, 2020; date of current version December 8, 2020. This work was supported in part by the National Natural Science Foundation of China under Grants 11704409, 61605246 and 61911530134, in part by Huo Yingdong Education Foundation under Grant 151062, and in part by Hunan Innovative Province Construction Project under Grant 2019RS3017. Corresponding author: Tianfu Yao (e-mail: yaotianfumary@163.com).

Abstract: In this paper, we study the thermal dissipation of Raman fiber laser and amplifier utilizing pure passive fiber as gain medium for the first time. Take into account the convective and conductive heat transferring process in the fiber, we consider the heat transferring and Raman conversion model based on the thermal conduction equations and the Raman coupled equations in the fiber. With the simulation of power distribution, the thermal profiles of Raman fiber laser are analyzed, including the transverse and longitudinal distributions of the heat load density, temperature, and thermal-induced refractive index change in the fiber. Meanwhile, the heat dissipation in multimode graded-index fiber and step-index fiber are also calculated and compared. The results show that the amplifier is superior to the resonator in heat alleviation, and the forward pumping scheme is also better to ease the thermal load than the backward and bidirectional pumping schemes, which have consult meaning for the suppression of thermal effects and the power scaling in Raman fiber lasers.

Index Terms: Fiber lasers, laser amplifiers, fiber non-linear optics, fiber optics systems.

1. Introduction

High power fiber lasers (HPFLs) are currently under intense investigations benefiting from eminent advantages such as good beam quality, high conversion efficiency, small footprint and excellent reliability [1], [2]. Thanks to the gradual availability of high-brightness Laser diodes (LDs), robust high-power fiber components and novel pumping schemes such as tandem pumping [3]–[6], the continuous-wave (CW) HPFLs have witnessed an exponential power increase and led to a variety of scientific and industrial applications [7], [8]. The primary implementation of HPFL is Ytterbium-doped fiber laser (YDFL) [9], [10], generating up to 10-kW near-diffraction-limited CW laser and beyond [11], [12].

Despite the impressive performances of high-power CW YDFLs, there are severe limitations for the further scaling of output power, among which thermal effect is considered as an important issue [13]–[17]. During the high-power operation, the quantum defect brings about the continuous temperature increment in the fiber core, causing thermal-optic effect and influencing the laser transmission. This is even worse when the large mode area (LMA) fiber is commonly employed

in the high-power laser systems to increase nonlinear threshold and scale the output power. Due to the excitation and amplification of high-order modes in the LMA fiber, the accumulated heat load would ultimately result in the energy transferring between various modes and lead to mode instability (MI), challenging the further power scaling of lasers [18], [19]. Accordingly, numerous researches have studied the heat dissipation problems in YDFLs theoretically and experimentally, such as the influences of pump directions or pump distributions [20]–[22], and the packing structure of the fiber [23]. Based on the analytical results, high-power experiments have been carried out with resonator [24] and amplifier configurations [25], discussing the cooling methods including air cooling or copper heat sink.

By contrast, Raman fiber lasers (RFLs) that utilize SRS effect can be an effective choice for high-power and wavelength-agile laser generation [26]–[31]. The intrinsic advantages include not only absence of parasitic lasing or photo darkening, but also lower quantum defect and eased thermal effects. Consequently, although the thermal distribution of the YDFLs has been widely calculated in pertinent literatures by solving thermal conduction equations, there are few reports discussing the heat dissipation in RFLs. So far, the power of RFLs has been promoted to a brand-new level, and up to 2-kW Raman fiber amplifier (RFA) has been reported utilizing multimode graded-index (GRIN) passive fiber [32]. Albeit with low quantum defect, the accumulated heat load in the fiber core is hard to dissipate at this high-power level. Thus the output performance of the RFL is severely influenced, resulting in fluctuation of beam spot and worsening of beam quality. Meanwhile, the temperature of fiber is so high that the polymer coating of the fiber would be damaged with scaled power. Some literatures have investigated MI originated from SRS and the heat load in RFL systems [33]–[36]. Hence, it is also necessary to quantitatively analyze the heat distribution in the high-power single-mode and multimode RFL system, which will be significant in the temperature estimation and the corresponding designing of cooling strategies to suppress MI and scale the output power.

In this paper, we study the thermal dissipation and power distribution in the RFL and RFA system based on pure passive fibers. By solving the thermal conduction equations and the Raman coupled equations, the transverse and longitudinal distributions of the heat load density, temperature, and refractive index in the fiber are calculated. Meanwhile, the heat dissipation characteristics in the fiber with various refractive index profiles, such as GRIN fiber and step-index (SI) fiber, are also analyzed and compared. The simulation shows that the amplifier is superior to the resonator according to heat alleviation, and the forward pumping scheme is also beneficial to ease the thermal load than the backward and bidirectional pumping schemes. This is the first demonstration of thermal analysis of RFL system, which offers insight into the thermal effect suppression and further power scaling of RFLs.

In Section 2, we begin with the conventional model of Raman fiber amplifier and resonator configurations. By analyzing the Raman coupling equations and heat conduction equations, we derive explicit expressions for the thermal distributions in the core, cladding and coating in Raman fiber laser systems. Then in Section 3, we simulate and compare the results in several cases, including the resonator and amplifier configurations, various pump directions, and different distributions of refractive index. In Section 4, the conclusions will be drawn.

2. Method and Model for Thermal Analysis

2.1 Raman Coupling Equations

Fig. 1(a) and (b) show the typical structures of the RFL and RFA respectively. The resonator scheme in Fig. 1(a) consists of a pair of high-reflectivity (HR) and low-reflectivity (LR) fiber Bragg gratings (FBGs) on both ends of the fiber (R_1 for longitudinal coordinate $z = 0$ and R_2 for $z = L_0$, L_0 is the fiber length), whilst there is no reflector in the amplifier in Fig. 1(b).

In the RFL system, we only consider the Raman conversion of pump, signal and 2nd order Stokes light. Based on this model, the Raman coupled equations of single mode RFL system can be

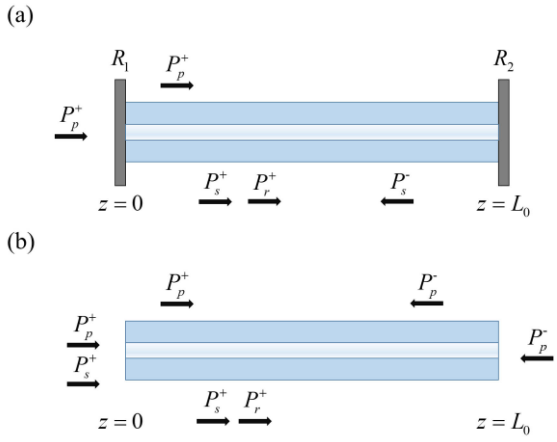

Fig. 1. The schematic structures of RFL (a) and RFA (b).

described by [37]:

$$\frac{dP_p^{\pm}(z)}{dz} = \mp \frac{\lambda_s}{\lambda_p} \frac{g_R}{A_{eff}} P_p^{\pm}(z)[P_s^+(z) + P_s^-(z)] \mp \alpha_p P_p^{\pm}(z) \tag{1}$$

$$\frac{dP_s^{\pm}(z)}{dz} = \mp \frac{\lambda_r}{\lambda_s} \frac{g_R}{A_{eff}} P_s^{\pm}(z)[P_r^+(z) + P_r^-(z)] \pm \frac{g_R}{A_{eff}} P_s^{\pm}(z)[P_p^+(z) + P_p^-(z)] \mp \alpha_s P_s^{\pm}(z) \tag{2}$$

$$\frac{dP_r^{\pm}(z)}{dz} = \pm \frac{g_R}{A_{eff}} P_r^{\pm}(z)[P_s^+(z) + P_s^-(z)] \mp \alpha_r P_r^{\pm}(z) \tag{3}$$

where P is the laser power, and λ is the wavelength of laser. The subscripts p, s and r represent the pump, signal, and 2nd Stokes laser, respectively. The superscript $+$ and $-$ represent the forward and backward propagating directions. g_R is the Raman gain coefficient, A_{eff} is the effective area for the Stokes conversion, here it equals the area of fiber core. α is the coefficient of background loss per unit length. The equations can be solved subject to the boundary conditions as follows:

$$P_p^+(0) = P_p^{in}(0) \tag{4}$$

$$P_p^-(L_0) = P_p^{in}(L_0) \tag{5}$$

$$P_s^+(0) = P_s^{in} + R_1 \times P_s^-(0) \tag{6}$$

$$P_s^-(L_0) = R_2 \times P_s^+(L_0) \tag{7}$$

In these equations, $P_p^{in}(0)$ and $P_p^{in}(L_0)$are the forward and backward launched pump power, and P_s^{in} is the forward-launched seed laser power. R_1 and R_2 are the reflectivity of HR and LR FBGs, respectively. The central wavelength of the FBGs is in accordance with the signal laser to enhance the reflection and the Raman conversion. For the amplifier structure, the reflectivity R_1 and R_2 equal to zero. Meanwhile, P_s^{in} in the resonator also equals to zero.

In the optical fiber with large mode field diameter (MFD) such as the multimode SI and GRIN fiber, the laser usually propagates in different modes. In the case of weak-coupling case, these modes enable various distributions of mode field and power, and the power conversion between different modes of pump and signal light are independent. Thus, the power considering every single

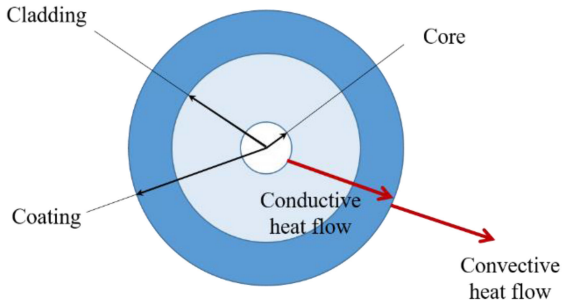

Fig. 2 Heat dissipation model of the fiber in RFL.

mode in the Raman laser can be written as:

$$\frac{dP_p^{\pm}(z,l)}{dz} = \mp\frac{\lambda_s}{\lambda_p} P_p^{\pm}(z,l)\sum_{m=1}^{M}\frac{g_R(\lambda_p,\lambda_s,l,m)[P_s^{+}(z,m)+P_s^{-}(z,m)]}{A_{eff}(\lambda_p,\lambda_s,l,m)} \mp \alpha_p(l)P_p^{\pm}(z,l) \tag{8}$$

$$\frac{dP_s^{\pm}(z,m)}{dz} = \mp\frac{\lambda_r}{\lambda_s} P_s^{\pm}(z,m)\sum_{n=1}^{N}\frac{g_R(\lambda_s,\lambda_r,m,n)[P_r^{+}(z,n)+P_r^{-}(z,n)]}{A_{eff}(\lambda_s,\lambda_r,m,n)}$$
$$\pm P_s^{\pm}(z,m)\sum_{l=1}^{L}\frac{g_R(\lambda_p,\lambda_s,l,m)[P_p^{+}(z,l)+P_p^{-}(z,l)]}{A_{eff}(\lambda_p,\lambda_s,l,m)} \mp \alpha_s(m)P_s^{\pm}(z,m) \tag{9}$$

$$\frac{dP_r^{\pm}(z,n)}{dz} = \pm P_r^{\pm}(z,n)\sum_{m=1}^{M}\frac{g_R(\lambda_s,\lambda_r,m,n)[P_s^{+}(z,m)+P_s^{-}(z,m)]}{A_{eff}(\lambda_s,\lambda_r,m,n)} \mp \alpha_r(n)P_r^{\pm}(z,n) \tag{10}$$

where l, m, and n are the l^{th}, m^{th}, and n^{th} mode in pump, signal and 2nd order Stokes laser, L, M, N are the corresponding sum amount of modes in the fiber. g_R/A_{eff} is the relative Raman gain coefficient between different modes with various wavelength, and A_{eff} can be represented based on the mode distributions [38]:

$$A_{eff}(\lambda_p,\lambda_s,l,m) = \frac{\iint|\varphi_p(x,y,l)|^2dxdy\iint|\varphi_s(x,y,m)|^2dxdy}{\iint|\varphi_p(x,y,l)|^2|\varphi_s(x,y,m)|^2dxdy} \tag{11}$$

In this equation, $\varphi_p(x,y,l)$ and $\varphi_s(x,y,m)$ are the transverse distribution of the pump mode l and signal mode m. Accordingly, the power distribution of single-mode or multimode RFL and RFA along the fiber can be calculated.

2.2 Heat Conduction Equations

As shown in Fig. 2 is the cross-section model of a core-pumped RFL. The radial distribution of the fiber includes the core, cladding and the coating. In this pumping scheme, the laser only propagates in the core of fiber. Thus, the heat is generated in the fiber core, then transferred gradually to the clad of the fiber through thermal conduction, and cooled by the outside environment through convection.

Due to the cylindrical structure of the fiber, the temperature distribution of fiber can be obtained from the steady-state heat equation for an isotropic medium [13]:

$$\nabla^2 T + \frac{Q}{\kappa} = 0 \tag{12}$$

where T is the temperature, Q is the generated heat density in per unit volume, and κ is the thermal conductivity. In the symmetrical structure, the azimuthal variation of temperature can be neglected.

Meanwhile, the fiber length in the RFL is generally more than tens of meters and far longer than its radial size, thus the z-variation is negligible compared with the r-variation. The heat source only generates in the core of the fiber in core-pumping scheme, thus Q is zero in the cladding and coating. Accordingly, the thermal conduction equations of the fiber can be written as:

$$\frac{1}{r}\frac{\partial}{\partial r}\left(r\frac{\partial T_1(r)}{r}\right)+\frac{Q}{\kappa_{core}}=0, 0\le r\le a_{core} \tag{13}$$

$$\frac{1}{r}\frac{\partial}{\partial r}\left(r\frac{\partial T_2(r)}{r}\right)=0, a_{core}\le r\le a_{clad} \tag{14}$$

$$\frac{1}{r}\frac{\partial}{\partial r}\left(r\frac{\partial T_3(r)}{r}\right)=0, a_{clad}\le r\le a_{coat} \tag{15}$$

In these equations, r is the radial coordinate, T_1, T_2, T_3 are the temperature of core, cladding and coating of the fiber. a_{core}, a_{clad} and a_{coat} are the radii of the core, cladding and coating, respectively. κ_{core}, κ_{clad} and κ_{coat} are the thermal conductivity of core, cladding and coating. Given that the thermal conduction between the various layers are perfect, the temperatures and the relative derivatives are continuous across the borders of different layers. Thus, the boundary conditions can be express as:

$$\left.\frac{dT_1(r)}{dr}\right|_{r=0}=0 \tag{16}$$

$$T_1(r)=T_2(r)\big|_{r=a_{core}}, \left.\frac{dT_1(r)}{dr}\right|_{r=a_{core}}=\left.\frac{dT_2(r)}{dr}\right|_{r=a_{core}} \tag{17}$$

$$T_2(r)=T_3(r)\big|_{r=a_{clad}}, \left.\frac{dT_2(r)}{dr}\right|_{r=a_{clad}}=\left.\frac{dT_3(r)}{dr}\right|_{r=a_{clad}} \tag{18}$$

In addition, on the surface of fiber coating, the temperature is determined by the convective heat flow, and the boundary condition is given by the Newton's law:

$$\left.\frac{dT_3}{dr}\right|_{r=a_{coat}}=\frac{h}{\kappa_{coat}}(T_4-T_3) \tag{19}$$

where T_4 is the coolant temperature, h is the convective heat transfer coefficient, describing the cooling at the surface of the fiber in contact with the outside cooling medium (i.e., h is $\sim$1000 W/(m^2·K) for water cooling method [13]). Thus the temperature of the different layers of the fiber can be derived by solving the thermal conduction equations subject to the boundary conditions as the following expressions:

$$T_1=T_4+\frac{Qa_{core}^2}{2ha_{coat}}+\frac{Q(a_{core}^2-r^2)}{4\kappa_{core}}+\frac{Qa_{core}^2}{2\kappa_{clad}}\ln\left(\frac{a_{clad}}{a_{core}}\right)+\frac{Qa_{core}^2}{2\kappa_{coat}}\ln\left(\frac{a_{coat}}{a_{core}}\right), 0\le r\le a_{core} \tag{20}$$

$$T_2=T_4+\frac{Qa_{core}^2}{2ha_{coat}}+\frac{Qa_{core}^2}{2\kappa_{clad}}\ln\left(\frac{a_{clad}}{r}\right)+\frac{Qa_{core}^2}{2\kappa_{coat}}\ln\left(\frac{a_{coat}}{a_{clad}}\right), a_{core}\le r\le a_{clad} \tag{21}$$

$$T_3=T_4+\frac{Qa_{core}^2}{2ha_{coat}}+\frac{Qa_{core}^2}{2\kappa_{coat}}\ln\left(\frac{a_{coat}}{r}\right), a_{clad}\le r\le a_{coat} \tag{22}$$

The thermal-optic effect in the fiber influences the actual refractive index, which can be calculated according to the equations of temperature distributions [13]:

$$n_T(r)=n_0+\beta\times\Delta T(r)=n_0+\beta\times[T(r)-T_4] \tag{23}$$

where n_T is the refractive index with thermal-induced change, and n_0 is the refractive index at temperature T_4. β is the thermal-optic coefficient, indicating the refractive index change per kelvin for different materials. Accordingly, the thermal-induced change of indices can be calculated, which is proportional to the heal load density Q.

In the Raman laser, the power enhancement is terminated when the 2nd order Stokes arises. Thus, the main heat source derives from the quantum defect based on Stokes conversion between pump and signal laser, and the background loss of the fiber. The heat density Q is found to be:

$$Q(z) = \frac{1}{A_{core}} \left[\begin{array}{c} \alpha_p [P_p^+(z) + P_p^-(z)] + \alpha_s [P_s^+(z) + P_s^-(z)] \\ + \left(\frac{\lambda_s}{\lambda_p} - 1 \right) \times \frac{g_R}{A_{eff}} [P_p^+(z) + P_p^-(z)] \times [P_s^+(z) + P_s^-(z)] \end{array} \right] \tag{24}$$

In terms of the power distribution of different modes, the Q can be expressed as:

$$Q(z) = \frac{1}{A_{core}} \left[\begin{array}{c} \sum_l^L \alpha_p(l) [P_p^+(z,l) + P_p^-(z,l)] + \sum_m^M \alpha_s(m) [P_s^+(z,m) + P_s^-(z,m)] \\ + (\frac{\lambda_s}{\lambda_p} - 1) \times \sum_l^L \sum_m^M \frac{g_R(\lambda_p, \lambda_s, l, m)}{A_{eff}(\lambda_p, \lambda_s, l, m)} [P_p^+(z,l) + P_p^-(z,l)] \times [P_s^+(z,m) + P_s^-(z,m)] \end{array} \right] \tag{25}$$

According to the above equations, the thermal and power distribution in the RFL system can be calculated.

3. Results and Discussions

In this section, we simulate and discuss the heat distribution in several cases, including the influence of configuration (resonator or amplifier), the pump directions (forward, backward and bidirectional pumping), and the refractive index distribution of fiber (GRIN or SI fiber).

3.1 Resonator and Amplifier Configurations

To compare the thermal load of RFL and RFA, we first consider a core-pumped Raman fiber resonator and its thermal profile. The values for the main parameters in the simulation are presented in Table 1. The employed SI fiber has core/cladding/coating radius of 15/62.5/100 μm, and the refractive index of core and cladding are 1.47 and 1.465, respectively. Accordingly, the V-number of the core is ~10, and the supported LP mode number is around 12. To simplify the calculation, we assume that the laser is in single-mode operation. In the practical experiment, the bend-induced modal loss can be employed to reduce higher-order modes and keep the single-mode output.

First, we compare the performance of a resonator and an amplifier using the same type of fiber, as is shown in Fig. 3. Note that the signal power increases more rapidly in the resonator than in the amplifier due to the multiple round trips within the cavity, and the 2nd order Raman laser grows faster and limits the growth of signal laser. With the same launched pump power, the fiber length is adjusted to balance the sufficient Raman conversion and the background loss of signal laser, hence the parameters of the cavity is optimized for comparison. The fiber length is 25 m, shorter than the 40 m length in the amplifier. In addition, the reflectivity of HR and LR FBGs are 99% and 10%, respectively.

As illustrated in Fig. 3(a) and (b), with the same launched pump power, the ultimate output signal laser at the end of the fiber in the resonator is slightly higher than that in the amplifier. Furthermore, their thermal distributions of heat load density and temperature along the fiber are quite different in Fig. 3(c) and (d). In the amplifier, the high temperature area concentrates on the middle portion of the fiber (z $\approx$ 18 m in this case), whilst the temperature is lower at the two ends of the fiber. By contrast, the temperature reaches the maximum at the input port of the resonator (z = 0), indicating the thermal pressure of HR FBG with high-power operation. Then the temperature decreases gradually towards the right end of the fiber (z = L_0). The maximum temperature of the amplifier is ~340 K, which is lower than the 402 K in the resonator. In Fig. 3(e) and (f), the high-temperature regions in both the resonant and amplifier schemes occupies the core of fiber. In the clad and coat layer of fiber, the temperature shows continuous decrease based on the cooling effect. Evidently, the propagation of laser in the fiber and the power distribution determine the thermal distribution.

Meanwhile, if the reflectivity of LR FBG is higher, the backward propagating signal laser power increases, resulting in higher power density as well as higher thermal load at the left end of the

TABLE 1
Physical Parameters and Values of Core Pumped RFL

Parameter	Value	Interpretation
λ_p	1080 nm	Pump wavelength
λ_s	1130 nm	Signal wavelength
λ_r	1185 nm	2nd Raman wavelength
α_p	0.001 /m	Loss of pump laser
α_s	0.001 /m	Loss of signal laser
α_r	0.001 /m	Loss of 2nd Stokes
K_{core} [13]	1.38 W/(m·K)	Thermal conductivity of core
K_{clad}	0.2 W/(m·K)	Thermal conductivity of clad
K_{coat}	0.2 W/(m·K)	Thermal conductivity of coat
h [13]	1000 W/(m^2·K)	Convective coefficient of water cooling
a_{core}	15 μm	Core radius
a_{clad}	62.5 μm	Cladding radius
a_{coat}	100 μm	Coating radius
$P_p^{in}(0)$	3500 W	Initial launched pump power
$P_s^{in}(0)$	30 W	Initial launched signal power
n_{core}	1.47	Refractive index of core
n_{clad}	1.465	Refractive index of clad
R_1	99%	Reflectivity of HR FBG
R_2	10%	Reflectivity of OC FBG
g_R [27]	5.3×10^{-14}	Raman gain coefficient

cavity. This result is also verified in our simulation. Thus, the decreasing reflectivity of LR FBG is beneficial to reduce the heat load of the resonator. To sum up, from the thermal point of view, the amplifier is more reliable with lower thermal load of the fiber devices.

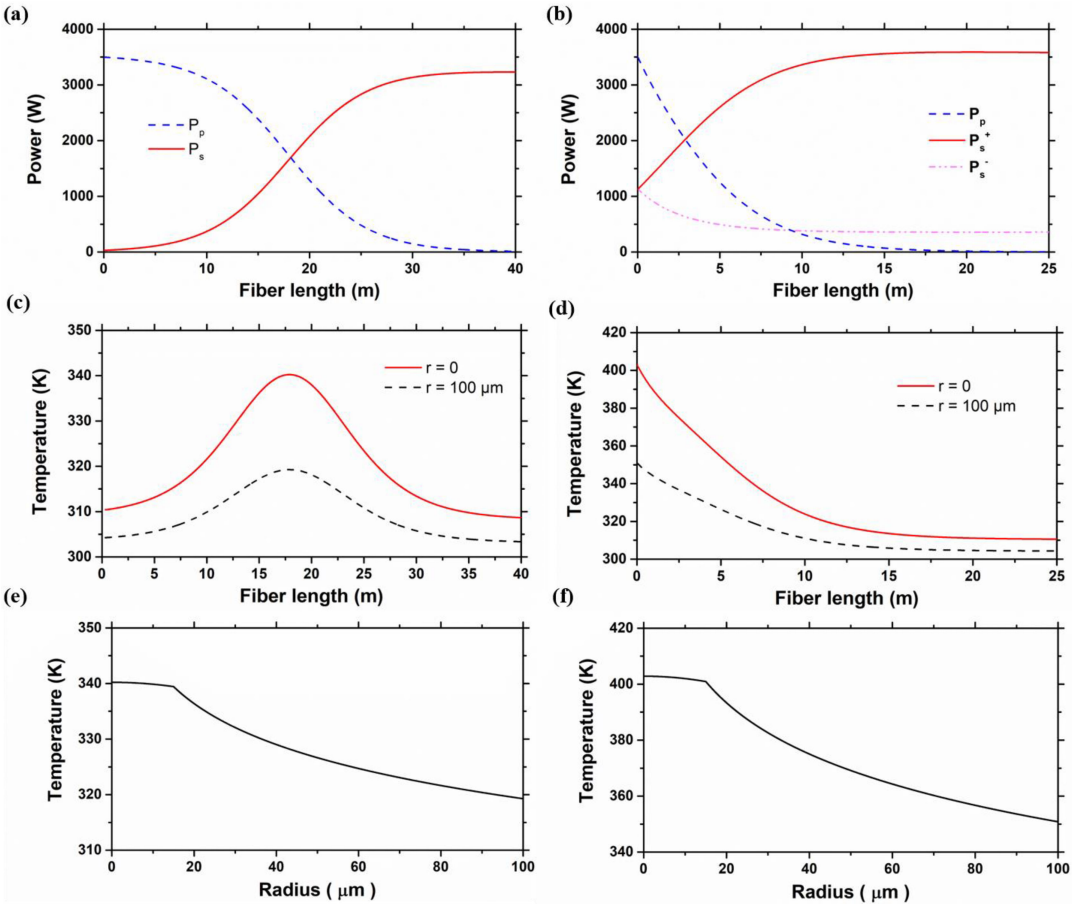

Fig. 3. The profiles of the resonator and amplifier, including the power distributions of amplifier (a) and the resonator (b), the temperature distributions along the fiber at the center of core and on the surface of the coat in the amplifier (c) and the resonator (d), and at the longitudinal position with maximum temperature, the temperature distributions in radial direction in the amplifier (e) and the resonator (f).

3.2 Pump Directions

To discuss the influence of pump direction on the thermal load, we simulate and compare the profiles of the backward and bidirectional pumped amplifiers. The results of backward pumped RFA is shown in Fig. 4. In the calculation, the signal laser increases more rapidly than the forward pumped one, thus the length of fiber is shortened to 20 m to suppress 2^{nd} order Stokes. The maximum output power at 1130 nm is 2854.2 W. In Fig. 4(a) and (b), due to the enhanced power density towards the output end of the fiber, the Raman conversion is more intense, resulting in the increasing temperature. The maximum temperature is ~427.6 K in the core of fiber ($z = 20$ m, $r = 0$), which is much higher than the forward pumping one. The temperature distribution in the radial direction is similar to that in Fig. 3(e), whilst the higher thermal load brings about more visible change of refractive index with an increase from 1.47 to 1.4713 in the core.

The evolutions of heat and power profiles in bidirectional pump scheme are also calculated, as shown in Fig. 5. In this case, the total pump power of 3500 W is injected from the two end of the gain fiber separately, with each of them of 1750 W. The fiber length is 40 m, and the maximum output power is 2961 W in Fig. 5(a). In Fig. 5(b) and (c), the heat load density of the fiber increases along the axial direction, and the maximum temperature of 375.3 K is attained in the center of core at the output port ($z = 40$ m, $r = 0$). Compared with the backward pumping RFA in Fig. 4(b),

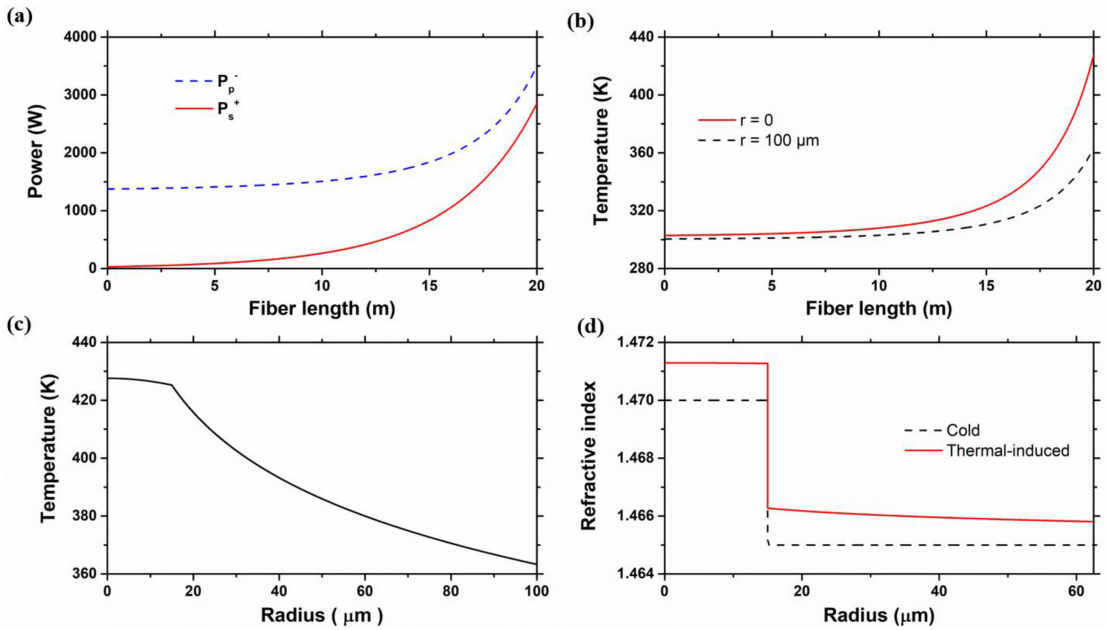

Fig. 4. The profiles of the backward pumped amplifier, including the power distributions of amplifier (a), the temperature distributions along the fiber of the center of core and the surface of the coat (b), and at maximum temperature, the temperature distributions in radial direction (c) and the thermal-induced refractive index change at maximum temperature (d).

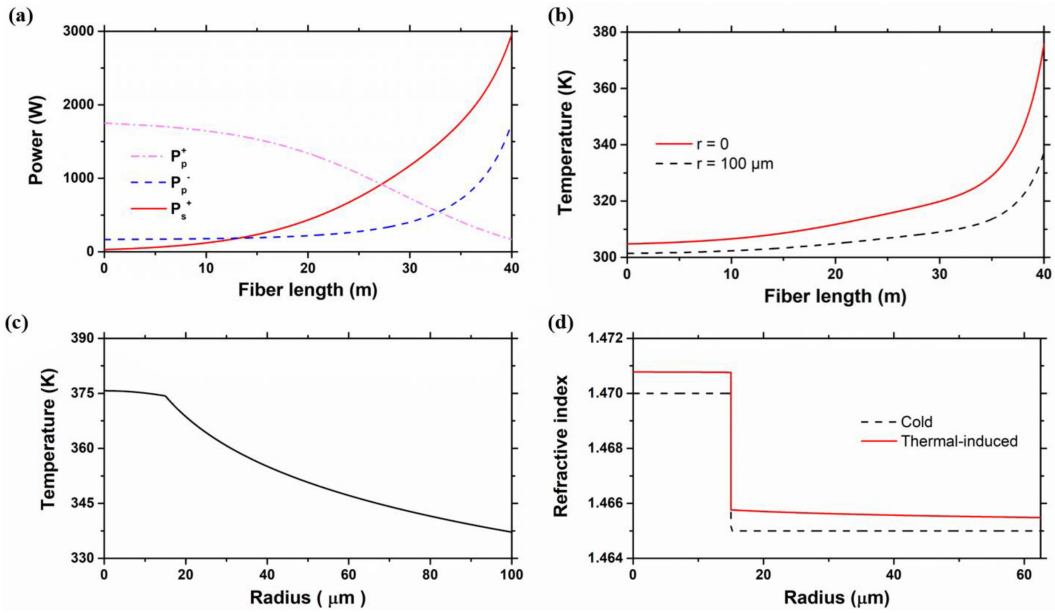

Fig. 5. The profiles of the amplifier with bidirectional pumping, including the power distributions of amplifier (a), the temperature distributions along the fiber at the center of core and on the surface of the coat (b), at maximum temperature, the temperature distributions in radial direction (c), and the thermal-induced refractive index change at maximum temperature (d).

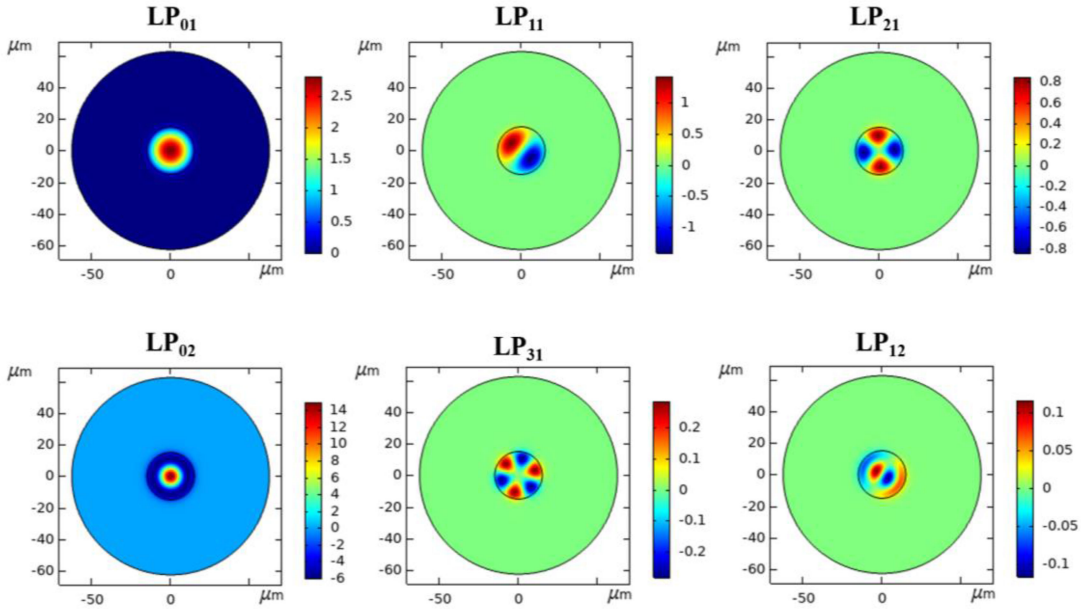

Fig. 6. The first 6 low-order modes and the energy distributions.

the power density near the output end is reduced in the bidirectional pumping scheme, thus the thermal load is relatively alleviated. In Fig. 5(d), the refractive index of the core increases from 1.47 to 1.4708 due to the thermal effects, and the thermal-induced index change is also smaller than that in Fig. 4(d).

In the case of the same total pump power and length of fiber, the output power of bidirectional pumped amplifier is lower than that in the forward pumped one. Accordingly, the power density of the amplified signal laser is lower, which may be beneficial to the suppression of 2nd order Stokes light. However, with the increasing portion of launched pump power in the backward direction, the heat load at the output end of fiber increases gradually. This is quite different from the thermal distribution in YDFLs. According to the gain scheme in YDFL, the thermal load is determined by the power density of pump laser, rather than the power density of signal laser [22]. Thus, through bidirectional pumping scheme and division of pump power, the heat load at the input fiber end can be eased effectively. However, in the RFL case, the thermal load is determined by both the pump and signal laser power, thus the backward or bidirectional pumped structure has higher thermal load than the forward pumped RFL. Therefore, the output port requires more efficient cooling strategy to avoid thermal damage of the end of the fiber.

3.3 Distribution of Refractive Index

After the calculation of single-mode fiber, we analyze the thermal profiles of RFA utilizing GRIN fiber, which is shown in Fig. 6. In this case, the refractive index of the fiber is:

$$n(r) = \begin{cases} n_0[1 - 2\Delta(\frac{r}{R_{core}})^2]^{\frac{1}{2}}, \Delta = \frac{NA^2}{2n_0^2}, r \le R_{core} \\ n_0[1 - 2\Delta]^{\frac{1}{2}}, R_{core} < r \le R_{clad} \end{cases} \tag{26}$$

Where n_0 is the refractive index at the center of the core, Δ is the relative refractive index, and NA is the numerical aperture. In the calculation, $n_0 = 1.47$, and $NA = 0.2$. The first 6 low-order modes and the corresponding energy profiles are shown in Fig. 6, leading to the similar thermal energy distributions.

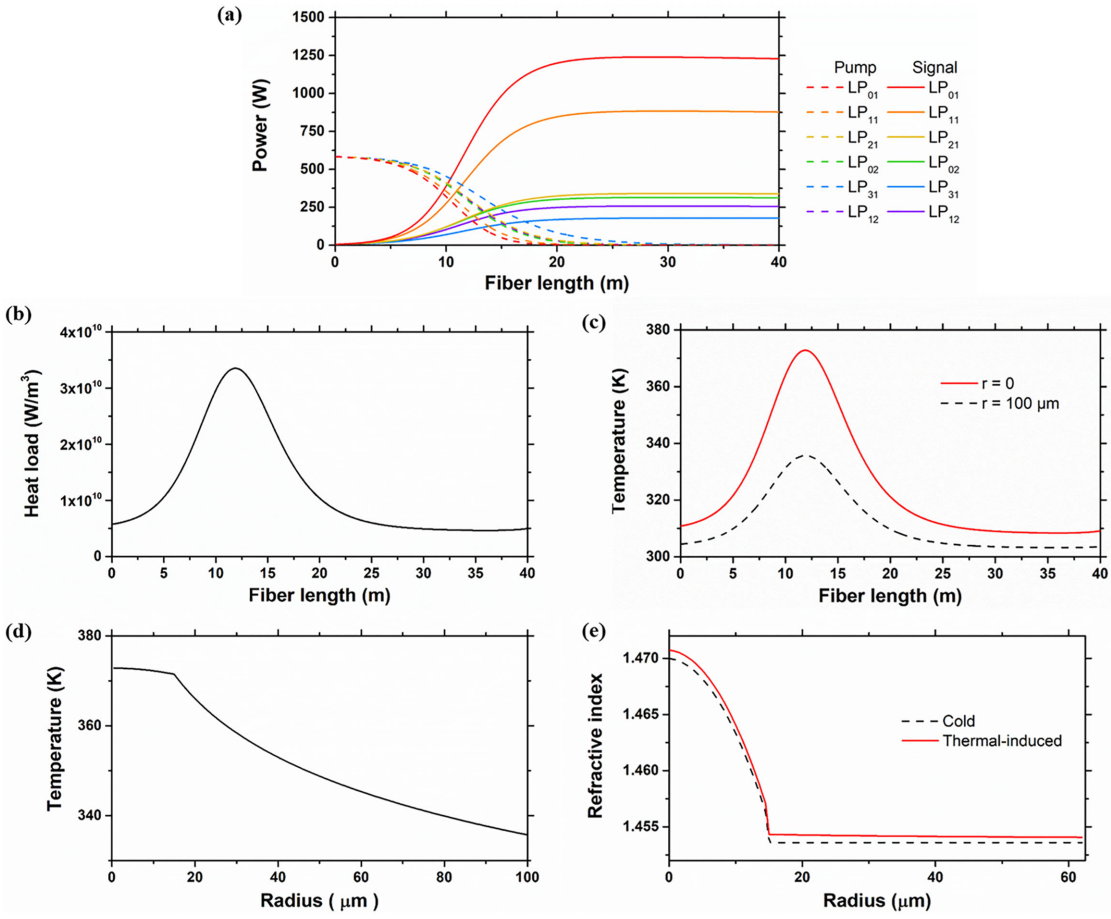

Fig. 7. The profiles of the core-pumped amplifier based on multimode GRIN fiber, including the power distributions of amplifier (a), the heat load density along the fiber (b), the temperature distributions along the fiber at the center of core and the surface of the coat (c), the temperature distributions in radial direction at maximum temperature (d), and the thermal-induced refractive index change at maximum temperature (e).

The relative Raman coefficients of high-order modes are much smaller than the fundamental mode. Thus, we simulate the power distribution of the first six low-order modes in the amplifier to simplify the calculation. The total pump and seed laser power are 3500 W and 30 W, respectively. Meanwhile, we assume that the power is distributed equally to each transverse mode. In Fig. 7(a), the LP_{01} mode in the signal light has the maximum gain, and it reaches the highest power at the end of the fiber. This also contributes to the beam cleanup effect in the GRIN fiber [39], [40]. The maximum of heat load density and temperature situate in the middle portion of the fiber in Fig. 7(b) and (c), with the maximum temperature of $\sim$372.8 K ($z \approx 12$ m). In Fig. 7(e), the thermal-induced refractive index in the core center with maximum heat load is increased to 1.4707.

We compare the thermal profiles of GRIN fiber and the ordinary SI fiber with the same 6 low-order modes, and the results in SI Raman fiber are shown in Fig. 8. The fundamental mode does not have the maximum Raman gain in this case. Instead, the Raman gain among the various modes are similar, and the corresponding power differences are smaller than that in the GRIN fiber. The maximum temperatures are 372.8 K and 345.1 K in GRIN and SI fiber, respectively. With this same pump distribution, the thermal load in SI fiber is smaller than that in the GRIN fiber, resulting in a smaller difference of thermal-induced refractive index.

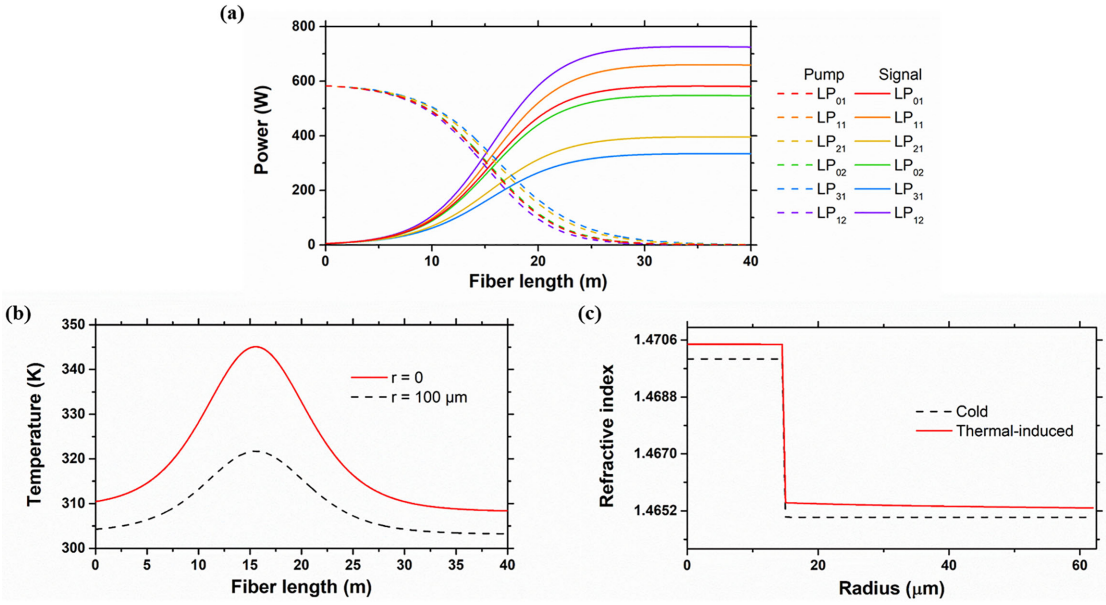

Fig. 8. The profiles of the core-pumped amplifier based on multimode SI fiber, including the power distributions of amplifier (a), the temperature distributions along the fiber at the center of core and the surface of the coat (b), and the thermal-induced refractive index change at maximum temperature (c).

4. Conclusion

To sum up, based on the heat transferring and Raman conversion model, a theoretical and numerical analysis of the thermal dissipation in high-power RFL and RFA utilizing passive fiber is investigated for the first time. The calculation employs thermal conduction equations and the Raman coupled equations considering the convective and conductive heat transferring in the fiber. We simulate the power distribution in resonator and amplifier with various pumping schemes and mode distributions. Accordingly, the transverse and longitudinal distributions of the heat load density, temperature, and refractive index in the fiber are analyzed. The results show that the SI fiber has smaller heat load than the GRIN fiber owing to the more even gain distribution. Meanwhile, the amplifier is superior to the resonator configuration in heat alleviation, and the forward pumping scheme is also beneficial to ease the thermal load than the backward and bidirectional pumping schemes. The theoretical results can provide guidance on the designing and cooling methods of RFL systems for the further power scaling.

References

[1] M. N. Zervas and C. A. Codemard, "High power fiber lasers: A review," *IEEE J. Sel. Topics Quantum Electron.*, vol. 20, no. 5, pp. 219–241, Sep./Oct. 2014.
[2] W. Shi, Q. Fang, X. Zhu, R. A. Norwood, and N. Peyghambarian, "Fiber lasers and their applications [Invited]," *Appl. Opt.*, vol. 53, no. 28, pp. 6554–6568, 2014.
[3] M. Werner, C. Wessling, S. Hengesbach, M. Traub, and H. D. Hoffmann, "100 W/100 μm passively cooled fiber coupled diode laser at 976 nm based on multiple 100 μm single emitters," in *Proc. SPIE*, vol. 7198, 2009, Art. no, 71980P.
[4] W. Mohammed and X. Gu, "Fiber bragg grating in large-mode-area fiber for high power fiber laser applications," *Appl. Opt.*, vol. 49, no. 28, pp. 5297–5301, 2010.
[5] D. Neugroschl, J. Park, M. Wlodawski, J. Singer, and V. Kopp, "High-efficiency $(6 + 1) \times 1$ combiner for high power fiber lasers and amplifiers," in *Proc. SPIE*, vol. 8601, 2013, Art. no. 860139.
[6] P. Zhou *et al.*, "High-power fiber lasers based on tandem pumping," *J. Opt. Soc. Am. B*, vol. 34, no. 3, pp. A29–A36, 2017.
[7] A. E. Willner *et al.*, "Optics and photonics: Key enabling technologies," *Proc. IEEE*, vol. 100, pp. 1604–1643, May. 2012.
[8] B. Shiner, "The impact of fiber laser technology on the world wide material processing market," in *CLEO: Applications and Technology*, AF2J.1, 2013.

[9] Q. Fang *et al.*, "5 kW near-diffraction-limited and 8 kW high-brightness monolithic continuous wave fiber lasers directly pumped by laser diodes," *IEEE Photon. J.*, vol. 9, no. 5, Oct. 2017, Art. no. 1506107.
[10] Y. Ye *et al.*, "Experimental study of 5 kW high stability monolithic fiber laser oscillator with or without external feedback," *IEEE Photon. J.*, vol. 11, no. 4, Aug. 2019, Art. no. 1503508.
[11] E. Stiles, "New developments in IPG fiber laser technology," in *Proc. 5th Int. Workshop Fiber Lasers*, 2009, pp. 4–9.
[12] X. Chen *et al.*, "Home-made 10 kW fiber laser with high efficiency," *Acta Optica Sinica*, vol. 39, no. 3, 2019, Art. no. 336001.
[13] D. Brown and H. Hoffman, "Thermal, stress, and thermo-optic effects in high average power double-clad silica fiber lasers," *IEEE J. Quantum Elect.*, vol. 37, no. 2, pp. 207–217, Feb. 2001.
[14] J. W. Dawson, M. J. Messerly, R. J. Beach, M. Y. Shverdin, and C. P. J. Barty, "Analysis of the scalability of diffraction-limited fiber lasers and amplifiers to high average power," *Opt. Exp.*, vol. 16, no. 17, pp. 13240–13266, 2008.
[15] J. Zhu, P. Zhou, Y. Ma, X. Xu, and Z. Liu, "Power scaling analysis of tandem-pumped Yb-doped fiber lasers and amplifiers," *Opt. Exp.*, vol. 19, no. 19, pp. 18645–18654, 2011.
[16] W. Ke, X. Wang, X. Bao, and X. Shu, "Thermally induced mode distortion and its limit to power scaling of fiber lasers," *Opt. Exp.*, vol. 21, no. 12, pp. 14272–14281, 2013.
[17] M. N. Zervas, "Transverse mode instability, thermal lensing and power scaling in Yb^{3+}-doped high-power fiber amplifiers," *Opt. Exp.*, vol. 27, no. 13, pp. 19019–19041, 2019.
[18] H. Otto *et al.*, "Temporal dynamics of mode instabilities in high-power fiber lasers and amplifiers," *Opt. Exp.*, vol. 20, no. 14, pp. 15710–15722, 2012.
[19] B. Ward, C. Robin, and I. Dajani, "Origin of thermal modal instabilities in large mode area fiber amplifiers," *Opt. Exp.*, vol. 20, no. 10, pp. 11407–11422, 2012.
[20] W. Yong, X. Chang-Qing, and P. Hong, "Thermal effects in kilowatt fiber lasers," *IEEE Photonic. Tech. L.*, vol. 16, no. 1, pp. 63–65, Jan. 2004.
[21] J. Li *et al.*, "Theoretical analysis of the heat dissipation mechanism in Yb^{3+}-doped double-clad fiber lasers," *J. Mod. Opt.*, vol. 55, no. 3, pp. 459–471, 2008.
[22] L. Huang *et al.*, "Towards the enhancement of the TMI threshold in monolithic high-power fiber system by controlling the pump distribution and the seed power," *IEEE Photon. J.*, vol. 10, no. 5, Oct. 2018, Art. no. 1504312.
[23] Y. Lv and S. Liu, "Heat dissipation model and temperature distribution of Yb-doped double-clad fiber in the composite system," *Opt. Fiber Technol.*, vol. 58, 2020, Art. no. 102269.
[24] P. Li *et al.*, "Theoretical and experimental investigation of thermal effects in a high power Yb^{3+}-doped double-clad fiber laser," *Opt. Laser Technol.*, vol. 40, no. 2, pp. 360–364, 2008.
[25] Y. Fan *et al.*, "Thermal effects in kilowatt all-fiber MOPA," *Opt. Exp.*, vol. 19, no. 16, pp. 15162–15172, 2011.
[26] V. R. Supradeepa, Y. Feng, and J. W. Nicholson, "Raman fiber lasers," *J. Opt.*, vol. 19, 2017, Art. no. 23001.
[27] Y. Feng, "*Raman Fiber Lasers*", Springer, Berlin, 2017.
[28] W. Yao, J. Liu, N. Chen, J. Zhang, Y. Zhao, and D. Shen, "Novel raman fiber lasers emitting in the U-band with combined volume bragg gratings," *IEEE Photon. J.*, vol. 6, no. 6, Dec. 2014.
[29] H. Zhang, P. Zhou, X. Wang, X. Du, H. Xiao, and X. Xu, "Hundred-watt-level high power random distributed feedback raman fiber laser at 1150 nm and its application in mid-infrared laser generation.," *Opt. Exp.*, vol. 23, no. 13, pp. 17138–17144, 2015.
[30] J. Xu *et al.*, "Incoherently pumped high-power linearly-polarized single-mode random fiber laser: Experimental investigations and theoretical prospects," *Opt. Exp.*, vol. 25, no. 5, pp. 5609–5617, 2017.
[31] Z. Wang *et al.*, "Dual-wavelength bidirectional pumped high-power raman fiber laser," *High Power Laser Sci.*, vol. 7, 2019, Art. no. e5.
[32] Y. Chen, T. Yao, L. Huang, H. Xiao, J. Leng, and P. Zhou, "2 kW high-efficiency raman fiber amplifier based on passive fiber with dynamic analysis on beam cleanup and fluctuation," *Opt. Exp.*, vol. 28, no. 3, pp. 3495–3504, 2020.
[33] H. Zhang, H. Xiao, X. Wang, P. Zhou, and X. Xu, "Mode dynamics in high-power yb-raman fiber amplifier," *Opt. Lett.*, vol. 45, no. 13, pp. 3394–3397, 2020.
[34] S. Naderi, I. Dajani, J. Grosek, and T. Madden, "Theoretical and numerical treatment of modal instability in high-power core and cladding-pumped raman fiber amplifiers," *Opt. Exp.*, vol. 24, no. 15, pp. 16550–16565, 2016.
[35] V. Distler, F. Möller, M. Strecker, G. Vega, T. Walbaum, and T. Schreiber, "Transverse mode instability in a passive fiber induced by stimulated raman scattering," *Opt. Exp.*, vol. 28, no. 15, pp. 22819–22828, 2020.
[36] Z. Li *et al.*, "Impact of stimulated raman scattering on the transverse mode instability threshold," *IEEE Photon. J.*, vol. 10, no. 3, Jun. 2018, Art. no. 1502709.
[37] G. P. Agrawal, *Nonlinear Fiber Optics*, 4th ed., San Diego, USA: Academic Press, 2006.
[38] J. Ji, C. A. Codemard, and J. Nilsson, "Analysis of spectral bendloss filtering in a cladding-pumped W-type fiber raman amplifier," *J. Lightw. Technol.*, vol. 28, no. 15, pp. 2179–2186, 2010.
[39] N. B. Terry, T. G. Alley, and T. H. Russell, "An explanation of SRS beam cleanup in graded-index fibers and the absence of SRS beam cleanup in step-index fibers," *Opt. Exp.*, vol. 15, no. 26, pp. 17509–17519, 2007.
[40] A. Polley and S. E. Ralph, "Raman amplification in multimode fiber," *IEEE Photonic. Tech. L.*, vol. 19, no. 4, pp. 218–220, Feb. 2007.